applied sciences

MDPI

*Article*

# Laser-Assisted Etching of EagleXG Glass by Irradiation at Low Pulse-Repetition Rate

**Roberto Memeo [1,2], Mattia Bertaso [1], Roberto Osellame [2], Francesca Bragheri [2] and Andrea Crespi [1,2,*]**

[1] Dipartimento di Fisica, Politecnico di Milano, p.za Leonardo da Vinci 32, I-20133 Milano, Italy; roberto.memeo@polimi.it (R.M.); mattia.bertaso@mail.polimi.it (M.B.)
[2] Istituto di Fotonica e Nanotecnologie, Consiglio Nazionale delle Ricerche (IFN-NCR), p.za Leonardo da Vinci 32, I-20133 Milano, Italy; roberto.osellame@ifn.cnr.it (R.O.); francesca.bragheri@ifn.cnr.it (F.B.)
* Correspondence: andrea.crespi@polimi.it

**Abstract:** Femtosecond laser micromachining is becoming an established technique for the fabrication of complex three-dimensional structures in glass. The combination of laser writing and chemical etching increases the technique versatility by allowing the fabrication of hollow structures within the bulk material. The possibility to encompass both optical and fluidic components in a single substrate allows us to realize optofluidic devices usable in several application fields. Here, we present new investigations of laser-assisted etching in Eagle XG glass showing good etching conditions at low repetition rates, where thermal effects can be neglected, and low irradiation speeds, which allow for complex microchannel network formation.

**Keywords:** laser-assisted etching; femtosecond laser micromachining; alumino-borosilicate glass



**Citation:** Memeo, R.; Bertaso, M.; Osellame, R.; Bragheri, F.; Crespi, A. Laser-Assisted Etching of EagleXG Glass by Irradiation at Low Pulse-Repetition Rate. *Appl. Sci.* **2022**, *12*, 948. https://doi.org/10.3390/app12030948

Academic Editor: István B Földes

Received: 15 December 2021
Accepted: 14 January 2022
Published: 18 January 2022



## 1. Introduction

Femtosecond Laser Micromachining (FLM) is a highly-versatile technique for the rapid prototyping of integrated devices in dielectric substrates [1]. In this technique, focused femtosecond laser pulses are exploited to obtain permanent and localized modifications of the material, limited to the focal region. Hence, by translating the substrate relatively to the laser focus, it is possible to inscribe complex three-dimensional geometries directly inside the bulk material, without affecting the surface and in a completely maskless approach.

FLM enables a wide portfolio of microstructuring possibilities, which can be accessed by proper tuning of the irradiation parameters and the correct choice of substrate. In particular, in many dielectric substrates it is possible to tune the irradiation parameters to obtain smooth refractive index changes, enabling the direct inscription of optical waveguides as 3D paths in the bulk [2]. In a more restricted subset of substrates, including fused silica [3–5] and photosensitive glasses [6], the irradiated tracks can yield a higher etching rate than the pristine material, when exposed to chemical agents such as aqueous solutions of hydrofluoric acid (HF) or potassium hydroxide (KOH). The latter feature is exploited to realize buried microchannels and hollow 3D microstructures inside the bulk material, in a method known as laser-assisted etching or FLICE (Femtosecond Laser Irradiation followed by Chemical Etching).

Fused silica is indeed a widely adopted substrate for FLM. In fused silica, the etching rate of laser-irradiated tracks can be hundreds of times higher than the one of the bulk material [5], allowing for the microstructuring of buried microchannels with very high aspect ratios. By combining optical waveguides and microchannels, fabricated with a single irradiation step, it is possible to realize compact optofluidic devices where the fluidic and the optical parts are intrinsically aligned with high precision [7]. Along this line, diverse optofluidic labs-on-chips, realized by FLM in fused silica substrates, have been reported in recent years, with applications ranging from cellomics [8] to microrheology [9] and quantum metrology [10]. Nonetheless, achieving low-loss optical waveguides and high

refractive index contrast in a fused silica substrate is not a trivial task, requiring special fabrication techniques and long fabrication times [11–13]. This impacts on the overall design complexity of integrated optofluidic devices realized by FLM.

On the other hand, waveguides with high index contrast and low propagation losses have been demonstrated in commercial borosilicate glasses, such as Eagle2000 and EagleXG (Corning Inc., Corning, NY, USA) [14–16] or AF45 (Schott AG, Mainz, Germany) [17]. These have enabled the demonstration of elaborated 3D optical circuits with applications encompassing quantum information experiments [18,19], astrophotonics [20], and telecommunications [21]. The application of the FLICE microstructuring technique to these glasses would disclose a great potential for the fabrication of optofluidic devices, where complex interferometers [18,22] could be integrated monolithically with a microfluidic network.

Laser-assisted etching in borosilicate glasses has been marginally investigated to date. First studies failed to find relevant etching selectivity of the laser-irradiated tracks in these substrates [4]. More recently, laser-assisted etching with HF and KOH was demonstrated in EagleXG glass [23], but by adopting very high scan speeds for the laser irradiation (in the order of 50–100 mm/s), which can be problematic in the inscription of minute details or when using advanced shape-control techniques [24]. Other works assessed favourable etching selectivity in KOH solutions for Pyrex (Corning 7740) [25] and Borofloat 33 (Schott) [26] glass; however, complex optical circuits have not been demonstrated, as to now, in these substrates by FLM.

In this work, we advance the experimental investigation of the FLICE technique in the EagleXG (Corning) glass, employing both HF and KOH etching solutions. By exploring a large set of irradiation parameters, we find convenient conditions showing high etching selectivity, for a pulse repetition rate of 25 kHz and translation speeds in the order of 1 mm/s, which are compatible with the inscription of elaborated patterns.

## 2. Materials and Methods

The adopted source is an Ytterbium laser (Pharos, Light Conversion, Vilnius, Lithuania), consisting in a mode-locked oscillator followed by an amplifier. This system delivers 190-fs duration pulses at 1030-nm wavelength, with a maximum output power of 10 W and a tunable repetition rate up to 1 MHz. In the experiments discussed in this work, we fix the repetition rate of the amplifier section to 1 MHz and, unless specified differently, we set the internal pulse-picker to produce an output pulse-train at 25 kHz. In our microfabrication apparatus, the pulse energy $E_p$ used for irradiation is finely tuned by an attenuation stage, consisting of a half-waveplate followed by a linear polariser. An additional half-waveplate is used to control the impinging laser polarisation, keeping it parallel or orthogonal to the writing direction. The laser beam is finally focused in the EagleXG glass samples by a 40× (NA = 0.75) water-immersion objective, at 500 µm depth from the surface. The maximum available pulse energy, measured before the focusing objective, is 8.6 µJ. The glass sample is fixed onto a three-axis air-bearing translation stage (ABL1500, Aerotech Inc, Pittsburgh, PA, USA), allowing smooth motion and translation speeds $v_t$ up to 300 mm/s, while maintaining precision in positioning better than 10 nm.

Wet chemical etching of the irradiated samples is performed with two different etching agents: HF or KOH. In the first case, the glass sample is immersed in a beaker containing an aqueous solution of HF at 10% concentration; the beaker is then placed in an ultrasonic bath, which also keeps the temperature constant at 35 °C. The high etching rates achievable with HF make this chemical agent particularly convenient for a fast and efficient investigation of the etching process. In the second case, we use an aqueous solution of KOH at 10 M; during the etching process, the beaker is kept on a hotplate set at 90 °C, and a magnetic stirrer is used to continuously mix the solution. In this work, we do not investigate the dependence of the etching selectivity on the etchant concentration; the chosen concentrations of HF and KOH (reported here above) are comparable to those typically used in the literature to study laser-assisted etching of glass materials (see e.g., Refs. [3,5,7,23,25]).

For the characterization of the etched structures, we use an optical microscope (DM2700M, Leica, Wetzlar, Germany), equipped with a computer-connected CCD camera (PL B623CU, Pixelink, Ottawa, Canada). With the aid of a properly calibrated image-acquisition software, it is possible to take accurate dimensional measurements of the fabricated structures.

## 3. Experimental Results

### 3.1. Analysis of the Irradiation Parameters

In our previous work [23], we found good working conditions for laser-assisted etching of EagleXG glass at 1 MHz repetition rate and scan speeds >50 mm/s, while lower speeds were ineffective in achieving favourable etching selectivity. We note that, at that repetition rate of the laser pulses, relevant thermal accumulation effects are present in the irradiation process, which affect the material modification [14].

Here, we aim to assess the existence of a suitable range of irradiation parameters, which provides good selectivity while keeping the scan speed in the order of a few millimetres per second. Hence, we attempt the investigation of a totally different irradiation regime, for which the temporal separation between two subsequent pulses is sufficiently large to avoid heat build-up in the material. In detail, as the threshold for the onset of thermal accumulation effects in similar glasses is typically placed around 200 kHz repetition rate [14], we select the much lower value of 25 kHz.

As a preliminary characterisation of the laser-assisted etching process at 25 kHz, a limited set of straight tracks was written in the substrate, with a coarse-grained sampling of the available pulse energies, and values for $v_t$ between 0.5 mm/s and 4 mm/s. In addition, each track was written with two laser polarisations, orthogonal and parallel to the translation direction. Indeed, in laser-assisted etching processes, a marked dependence of the etching selectivity on the polarisation direction of the irradiation laser beam is often observed. After the fabrication, the sample was cut in two pieces, transversally with respect to the tracks, and lateral facets were polished to optical quality. The two resulting samples were then etched, one in HF and the other in KOH, as detailed in Section 2.

Figure 1a gives a schematic representation of the laser-assisted etching process we adopt in our experiments. As the etchant preferably attacks the laser-irradiated tracks, hollow cones are excavated along these tracks, starting from the lateral facet of the sample exposed to the acid, as shown in Figure 1b. The aspect ratio (A.R.) of the cones, defined as the ratio of the length over the basis radius, is known to be approximately equal to the ratio of the etching rate of the irradiated track over the etching rate of the unmodified substrate [23] and it directly indicates the etching selectivity. Thus, after etching, the samples were characterized with the optical microscope, measuring the dimensions of the etched cones and calculating the A.R.s; results are reported in Figure 2.

As a matter of fact, to finely characterise the etching dynamics in the HF solution, each sample was etched in four successive steps of 5 min each, measuring the A.R. of the etched cones after each step. In fact, the changing equilibrium between chemical reaction and diffusion processes, inside the etched cone, can cause a decrease in the advancement rate of the tip of the cone, as it becomes longer [4,23]. This is typically observed as a sort of saturation of the length of the etched cone, and a decrease in the measured A.R., as the etching time increases. To calculate a reliable estimation of the etching selectivity in optimal conditions, it is appropriate to measure the A.R. of the cones at the shortest possible time, for which both the length and the radius of the cones can be measured accurately. In our experiments, this condition is met at 10 min, the etched cones still being too small after the first 5-min step. On the other hand, in the case of the KOH etching, which is a much slower process, we did not observe relevant saturation effects; the results plotted in Figure 2 refer to an etching time of 6 h.

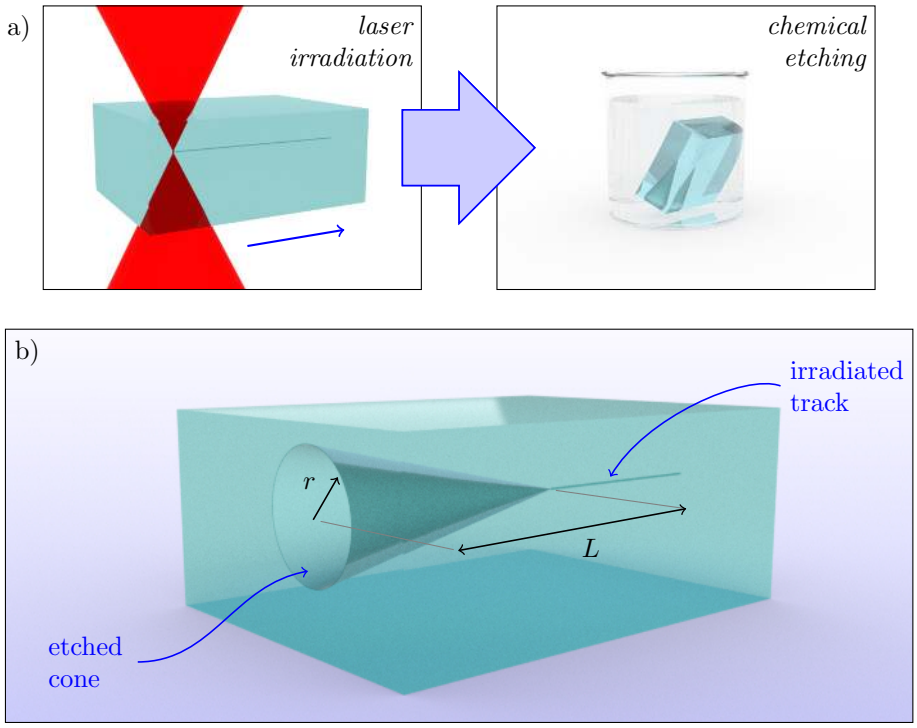


**Figure 1.** (**a**) Pictorial representation of the two steps of the laser-assisted etching process. First (**left panel**), tracks are irradiated with a focused femtosecond laser beam, in the bulk of a glass sample and covering its full length. The irradiation is performed by translating the sample at constant speed with respect to the laser focus. Second (**right panel**), the sample is immersed in a solution of HF or KOH for a controlled time. (**b**) Typical outcome of the etching process of a straight irradiated track. A hollow cone is formed along the track, with basis radius $r$ and length $L$. The aspect ratio (A.R.) of the cone, defined as A.R. $= L/r$, is a direct indication of the etching selectivity. Dimensions are not to scale.

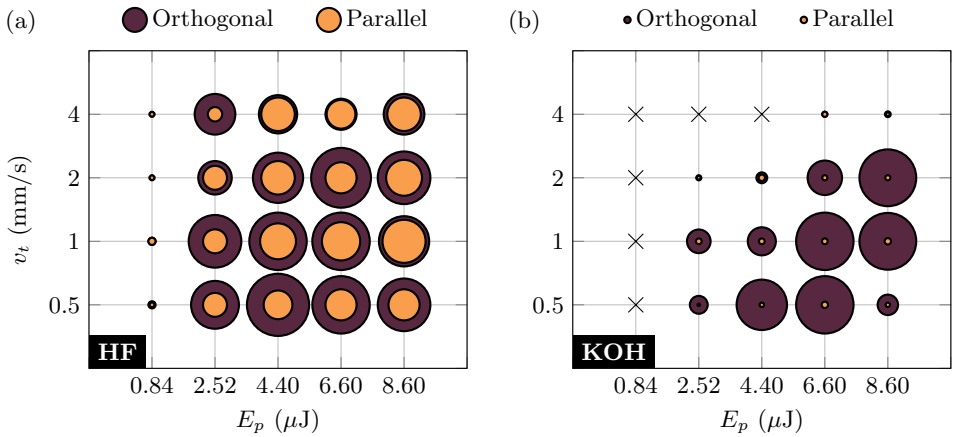


**Figure 2.** Characterisation of the A.R. of the etched cones as a function of the irradiation parameters: pulse energy $E_p$, translation speed $v_t$, and polarisation (parallel or orthogonal with respect to the translation direction). The repetition rate of the laser pulses is 25 kHz. The area of the coloured circles indicates the A.R. of the cones, as measured (**a**) after 10 min of etching in HF solution or (**b**) after 6 h in KOH solution. The size of the circles in the legend corresponds to a value of 10.

Little to no selectivity was observed for the lowest pulse energy ($E_p$ = 0.84 µJ), for both etchants, and independently of the adopted scan speed and polarisation. Significant etching selectivity was instead observed for the higher energies, though with different patterns in HF with respect to the KOH. In HF, we measured A.R.∼10–20 in a broad range

of parameters; the two polarisations give results that are in the same order of magnitude, even if the parallel one consistently provides slightly lower selectivity than the orthogonal one. On the other hand, in KOH the etching results are less uniform across the explored energies and speeds, and a clear dependence on the laser polarisation can be noticed. In particular, while the orthogonal polarization gives very high values of A.R. (up to about 90), the A.R. hardly reaches 10 for the parallel one.

On the basis of these preliminary results, we conducted a second experiment to better investigate the etching dynamics. In particular, we irradiated a set of tracks, performing a finer scan of the pulse energy between 0.6 µJ and 8.6 µJ, and with translation speeds again ranging from 0.5 mm/s to 4 mm/s. The polarisation of the writing beam was kept orthogonal to the translation direction, as it consistently provides the higher A.R. according to the first characterisation. For each couple of values of the parameters ($E_p$ and $v_t$), we wrote two identical tracks. After fabrication, the sample was cut into several pieces, whose lateral facets were polished, and which were later etched separately in HF and KOH solutions. Figure 3 plots the measured A.R. of the etched cones, after 10 min etching in case of HF and after 6 h in case of KOH.

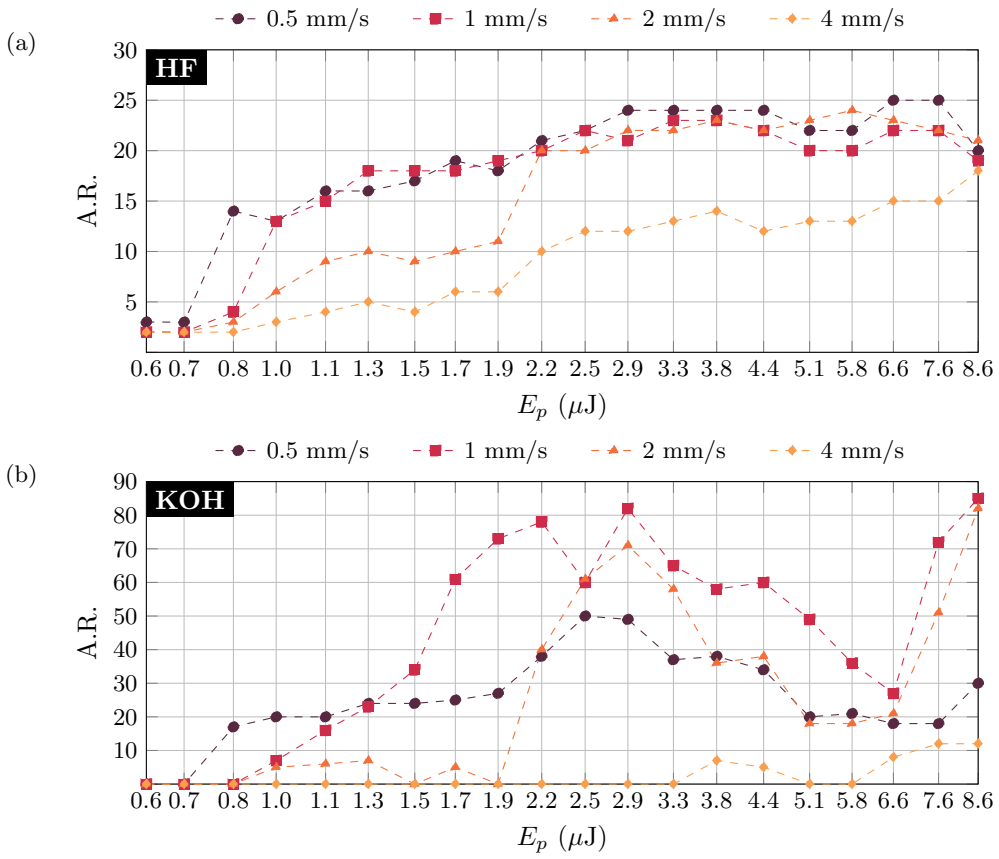


**Figure 3.** Measured A.R. of the etched cones, for tracks irradiated with different pulse energy $E_p$ and different translation speed $v_t$. Laser polarisation was kept orthogonal to the translation direction. The plotted values correspond to the averages of the measured A.R. of two different cones, obtained by tracks irradiated with identical parameters. Panel (**a**) refers to 10-min etching in HF solution, while panel (**b**) refers to 6-h etching in KOH solution.

A comparison between Figure 3a,b confirms the difference between the etching processes in the HF and KOH etchants, already visible in Figure 2. In detail, we observe that, in the case of HF etching, the measured A.R. at first increases with increasing pulse energy, then enters a sort of plateau in correspondence of $E_p \simeq 2$ µJ. For higher energies the A.R. remains practically constant, reaching maximum values around 25. This corresponds to an etching rate of the irradiated track of about 60 µm/min, namely 25 times larger than the

etching rate of the unmodified substrate 2.5 μm/min. Comparable results are achieved for all the explored scan speeds except for the highest one ($v_t$ = 4 mm/s), for which the A.R. is visibly lower, independently of the inscription power. On the other hand, in KOH the etching process seems to have a more complex dependence on the irradiation parameters, and the measured A.R. reaches optimal values only for selected combinations of $E_p$ and $v_t$. For $E_p \leq 2.9$ μJ, the A.R. of the etched cones increases with the energy, reaching a maximum value of about 80 for $v_t$ = 1 mm/s and $E_p$ = 2.9 μJ. For higher energies, 2.9 μJ $< E_p <$ 6.6 μJ, the A.R. drops and then increases again with the energy, reaching values around 80–85 for $E_p$ = 8.6 μJ and $v_t$ = 1–2 mm/s. The process is indeed very sensitive to the irradiation speed. It is worth noting that, whereas KOH enables higher selectivity than HF, the etching process in the KOH solution is much slower. In fact, in the latter case, the maximum etching rate of the irradiated track observed in our experiments is about 0.5–0.6 μm/min (the etching rate of the bulk substrate is about 0.008 μm/min).

### 3.2. Role of Thermal Effects

In the experimental study discussed in the previous Section, we chose the 25 kHz repetition rate as a reasonably low value to avoid thermal accumulation. In fact, the absence of thermal effects, in general, is not an absolute requirement in the laser-assisted etching technique, as convenient sets of irradiation parameters that provide good selectivity may also be found in the presence of these phenomena, with irradiation performed at high repetition rates [23,24]. However, the non-thermal regime can provide more versatility in adjusting the irradiation parameters, as the material modification is substantially independent of the timing of the pulses impinging in the focus. Namely, in this case, the same kind of modification can be obtained by keeping the pulse energy fixed, and by scaling both the repetition rate and the translation speed in such a way that the number of pulses per unit length of the irradiated track remains constant. Alternatively, the effect of a slower speed may be emulated by multiple overlapped laser scans. In addition, the absence of pulse-to-pulse cumulative effects makes the laser-matter interaction process simpler, and possibly facilitates its microscopic modelling.

To assess how widely the repetition rate can be varied, while maintaining the same non-thermal irradiation regime, we irradiated several tracks keeping the pulse energy $E_p$ constant, varying the repetition rate of the femtosecond laser from 5 kHz to 200 kHz, and scaling the translation speed $v_t$ proportionally. Two optimal sets of parameters, identified in the previous analysis at 25 kHz repetition rate, were chosen as references; in detail, $E_p$ = 2.2 μJ and $v_t$ = 1 mm/s, $E_p$ = 8.6 μJ and $v_t$ = 1 mm/s. All the tracks were written with orthogonal polarisation, as in the previously described results.

Figure 4a reports the cross-section of the irradiated tracks, imaged at the optical microscope after polishing the lateral facets of the glass substrate. Material modification from heat build-up is identified from the pictures as an elliptical white crown, which appears and then enlarges as the repetition rate increases. At the lowest pulse-energy explored ($E_p$ = 2.2 μJ), this feature is barely visible up to the highest repetition rate. On the other hand, for the highest pulse energy ($E_p$ = 8.6 μJ) it becomes evident already at 50 kHz.

After laser irradiation and polishing, the glass sample was immersed for 15 min in HF solution, and the A.R. of the etched cones was finally measured. Results are plotted in Figure 4b. We note that up to 25-kHz repetition rate the A.R. of the cones is almost constant for both values of $E_p$, consistently with the observation of no visible heat build-up. On the other hand, for higher repetition rates the A.R. changes, as thermal accumulation is altering the etching selectivity.

In the light of these results, we can conclude that, at the chosen repetition rate of 25 kHz, thermal accumulation effects are indeed small or negligible. In case it is needed for the application, it should be possible to further scale down the repetition rate together with the translation speed, down to 5 kHz, and reliably reproduce the results obtained at 25 kHz for a given pulse energy. Once in the single pulse regime, we expect that this scaling can be extended to even lower repetition rates, further reducing the translation

speed. On the contrary, caution should be used in performing an analogous scaling by increasing the repetition rate above 25 kHz. In fact, the onset of thermal accumulation effects may alter the laser-modification process and affect the etching selectivity. The results obtained in this work cannot be extended to repetition rates higher than 200 kHz in a straightforward fashion and dedicated experimental investigations should be performed to assess the etching selectivity in those regimes.

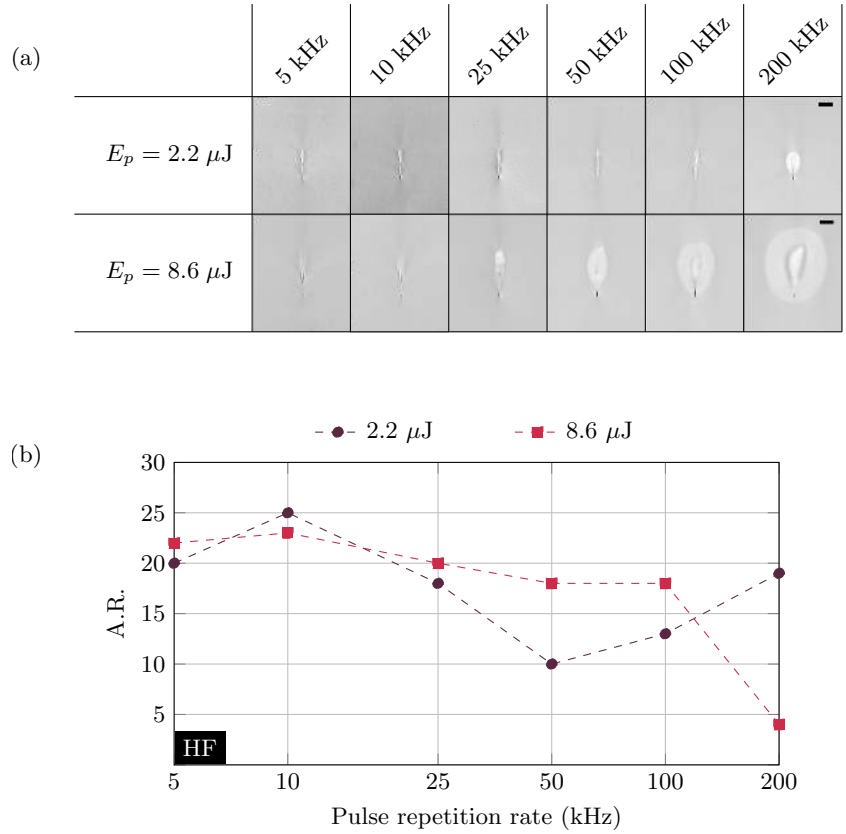


**Figure 4.** (**a**) Microscope pictures of the cross-section of tracks irradiated with two different values of $E_p$, and repetition rates ranging from 5 kHz to 200 kHz. Scalebars correspond to 5 μm (all pictures in the same row have the same scale). The scan speed is scaled proportionally to the repetition rate, keeping as reference $v_t$ = 1 mm/s at 25 kHz. (**b**) A.R. of the etched cones obtained from the above-illustrated tracks, as measured after 15 min immersion in HF solution.

### *3.3. Morphology of the Etched Structures*

In Figure 5, we report representative pictures of the etched cones, taken with the optical microscope, which reveal a difference in the smoothness of their surfaces as the irradiation energy increases. In fact, despite maintaining a high A.R., the cones corresponding to the highest irradiation pulse-energies (beyond 6.6 μJ) show a rougher surface after etching, if compared to the cones corresponding to lower energies, which are uniformly smooth for their whole length. This observation applies both to cones etched in HF and KOH solution. We note that this increase in roughness comes together with the rebound of the A.R. observed in Figure 3b for $E_P > 6.6$ μJ. This might be due to a different substrate modification process, which comes into play when the pulse energy surpasses a given threshold.

A smooth surface is preferable when dealing with the fabrication of microchannels for optofluidic circuits: a careful choice of the irradiation parameters should thus be made in order to match the requirements of the final device. A direct visual comparison of the roughness of the cones etched in HF or KOH is not easy, given the tiny diameter of the cones etched in KOH. In any case, it is worth noting that the quality of the unirradiated surfaces of the glass sample is also important in the applications, and we have observed

that this is indeed different after the exposure to the two etching agents. In fact, after immersion in HF solution, the surfaces that were polished to optical quality become slightly opaque and bumpy; on the contrary, such surface alterations are practically absent after KOH processing.

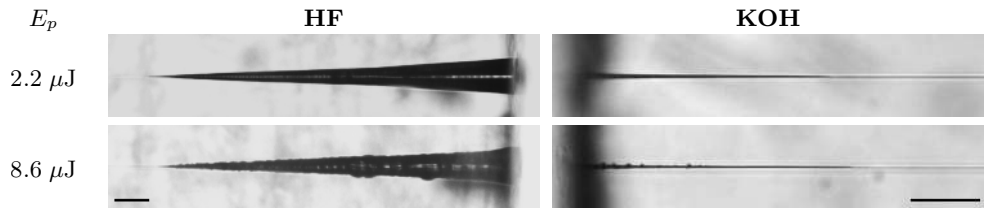


**Figure 5.** Examples of etched cones (top-view microscope pictures), obtained from tracks irradiated with orthogonal polarisation at two different inscription pulse-energies ($E_p$ = 2.2 µJ and $E_p$ = 8.6 µJ), $v_t$ = 1 mm/s and 25 kHz repetition-rate. Etching was performed in HF solution for 10 min or in KOH for 6 h. Scalebars correspond to 50 µm.

It is interesting to examine the inlet of the cones etched in KOH solution at the optical microscope (see the rightmost panels of Figure 6). In fact, it is clearly noted that, while the laser-modified region extends transversally for several microns, the chemical agent only attacks a practically point-like feature placed towards the bottom of the irradiated track. Indeed, even after several hours of immersion in the solution, the rest of the cross-section looks practically unaltered.

On the other hand, after several-minutes immersion in HF solution, the etched cone inlet is wider than the cross-section of the irradiated track (see, in particular, the pictures in Figure 6 corresponding to 10–20 min etching in HF). To gain further insight on the etching process in HF, we inscribed two sets of many identical tracks, corresponding to different irradiation parameters which give the best selectivity according to the data in Figure 3a, and observed how the excavation of the cones proceeds in small time steps. In detail, we inscribed tracks with laser polarization orthogonal to the writing direction, $v_t$ = 1 mm/s and either $E_p$ = 2.2 µJ or $E_p$ = 8.6 µJ. The sample was then cut in several pieces transversally to the tracks, the lateral facets were polished to optical quality, and pieces were immersed in HF solution for different times, up to 20 min.

By inspecting the cone inlets at the optical microscope (Figure 6), it is evident that also in the case of HF the etching proceeds from the same point-like feature in the lower part of the inscribed track. Here, however, the other regions of the modified cross-section also show some etching enhancement with respect to the bulk, though in a lesser measure. After longer etching times, the whole track results excavated, an elliptical cone inlet is formed and the initial inhomogeneity in the cross-section is no longer discernible.

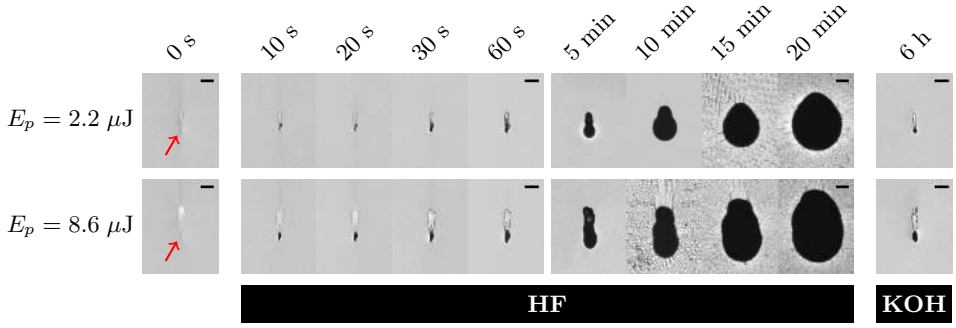


**Figure 6.** Microscope pictures of the cross-section of the irradiated tracks prior to etching (leftmost images), and after a different time of immersion in etching baths of HF or KOH. Red arrows point to the dark dots in the cross-section of the track, which corresponds to the point of maximum etching sensitivity. The two rows of images regard tracks written with two different values of $E_p$, $v_t$ = 1 mm/s and 25 kHz repetition rate. The length of the scalebars is 5 µm.

We note that a very similar behaviour, with the etching starting from a point-like feature in the cross-section modified track, was observed in our previous work [23] on the same glass EagleXG, despite the very different irradiation conditions. In particular, the point-like feature which yields enhanced etching rates corresponds to a small dark dot in the cross-section, visible with the optical microscope, which was identified as the location of the focal spot during irradiation [14].

Further investigations on the nature of this dark dot would be needed to fully explain the laser-assisted etching dynamics in this material. In any case, the interpretation of the black dot as a micro-crack propagating uniformly for the whole track length [23] seems compatible with the experimental findings of the increased surface roughness at high pulse energy (Figure 5). In fact, as the irradiation laser fluence increases, the modification undergone by the material may possibly become more and more disruptive and irregular.

The present results confirm substantial differences in the etching process occurring in EagleXG glass with respect to the case of pure fused silica. In fused silica, the whole cross-section of the laser-modified track is uniformly etched. Moreover, birefringent nanogratings, whose orientation depends on the polarisation direction of the inscribing laser, are observed in fused silica. These are deemed responsible for the polarisation dependency of the etching rates. In the experiments here described on EagleXG, we note that the etching process starts from a point-like structure formed in the focal spot of the writing laser, and it extends to the remaining track cross-section only for longer times. We also observed some polarisation dependency, but nanogratings were not noticeable. Further investigation on the morphology of the irradiated track at the microscopic level is needed to fully understand its complex etching behaviour.

## 4. Conclusions

We have demonstrated a new regime of laser-assisted etching in EagleXG glass substrate, with both HF and KOH etchants. Differently from previous work [23], where only high scan speeds for irradiation were found effective to induce etching selectivity, here we show that good working conditions can be achieved for about 1 mm/s scan speed at 25 kHz repetition rate. Best selectivity is observed with KOH etchant, reaching values above 80.

A low scan speed facilitates the irradiation of paths with tight curvatures, as required, for example, in the fabrication of microfluidic structures and to achieve precise control on the shape of the etched volumes [24].

We note that the two etchants provide different advantages and drawbacks, and one or the other may be adopted, depending on the application. For instance, KOH is suitable to realize hollow structures with high A.R. On the other hand, removal of large volumes of material may benefit from the lower selectivity and faster etching dynamics of HF.

We observe a polarization dependence of the etching selectivity, particularly pronounced in the case of KOH etchant. Nonetheless, nanogratings, responsible for polarization-dependent selectivity in fused silica [4], were not apparent in our experiments, and the etching process seems to be related to a point-like microscopic feature, akin to the one observed previously at 1 MHz repetition rate [23]. Additional studies are required on the microscopic origin of the laser-enhanced etching sensitivity in this material, which could explain the physical nature of the black dot in the cross-section, its authentic role in the etching process, and the dependence on the laser polarization.

We believe that this work opens the door to the effective use of EagleXG glass for optofluidic devices, fabricated by femtosecond laser writing followed by wet etching, as the low-repetition rate irradiation regime demonstrated here highly enhances the versatility of the process. In fact, in this regime, cumulative thermal effects are negligible, which means that scan speed and repetition rate can be adjusted together, keeping the same etching selectivity. In particular, the speed could be further lowered for inscribing details with higher accuracy, and set back to higher values to trace longer straight paths.

**Author Contributions:** R.M. and M.B. carried out the experimental activity. R.O., F.B. and A.C. conceived the work and supervised its development. All authors contributed to data analysis and to writing the paper. All authors have read and agreed to the published version of the manuscript.

**Funding:** A.C. acknowledges funding by the Italian Ministry of University and Research (PRIN 2017 progamme, QUSHIP project—id. 2017SRNBRK). F.B. acknowledges funding from EU under the European Union's Horizon2020 FET Open programme (PROCHIP project—grant agreement no.801336). R.O. acknowledges funding from the European Research Council (ERC) under the European Union's Horizon 2020 research and innovation programme (project CAPABLE—Grant agreement No. 742745).

**Institutional Review Board Statement:** Not applicable.

**Informed Consent Statement:** Not applicable.

**Data Availability Statement:** Raw data represented in the graphs of this manuscript are available from the corresponding author, upon reasonable request.

**Conflicts of Interest:** The authors declare no conflict of interest. The funders had no role in the design of the study; in the collection, analyses, or interpretation of data; in the writing of the manuscript, or in the decision to publish the results.

## References

1. Osellame, R.; Cerullo, G.; Ramponi, R. *Femtosecond Laser Micromachining: Photonic and Microfluidic Devices in Transparent Materials*; Springer Science & Business Media: Berlin/Heidelberg, Germany, 2012; Volume 123.
2. Della Valle, G.; Osellame, R.; Laporta, P. Micromachining of photonic devices by femtosecond laser pulses. *J. Opt. A Pure Appl. Opt.* **2009**, *11*, 013001. [CrossRef]
3. Bellouard, Y.; Said, A.; Dugan, M.; Bado, P. Fabrication of high-aspect ratio, micro-fluidic channels and tunnels using femtosecond laser pulses and chemical etching. *Opt. Express* **2004**, *12*, 2120–2129. [CrossRef]
4. Hnatovsky, C.; Taylor, R.; Simova, E.; Rajeev, P.; Rayner, D.; Bhardwaj, V.; Corkum, P. Fabrication of microchannels in glass using focused femtosecond laser radiation and selective chemical etching. *Appl. Phys. A* **2006**, *84*, 47–61. [CrossRef]
5. Kiyama, S.; Matsuo, S.; Hashimoto, S.; Morihira, Y. Examination of Etching Agent and Etching Mechanism on Femtosecond Laser Microfabrication of Channels Inside Vitreous Silica Substrates. *J. Phys. Chem. C* **2009**, *113*, 11560–11566. [CrossRef]
6. Cheng, Y.; Sugioka, K.; Midorikawa, K.; Masuda, M.; Toyoda, K.; Kawachi, M.; Shihoyama, K. Control of the cross-sectional shape of a hollow microchannel embedded in photostructurable glass by use of a femtosecond laser. *Opt. Lett.* **2003**, *28*, 55–57. [CrossRef]
7. Osellame, R.; Maselli, V.; Vazquez, R.; Ramponi, R.; Cerullo, G. Integration of optical waveguides and microfluidic channels both fabricated by femtosecond laser irradiation. *Appl. Phys. Lett.* **2007**, *90*, 231118. [CrossRef]
8. Bragheri, F.; Minzioni, P.; Vazquez, R.M.; Bellini, N.; Paie, P.; Mondello, C.; Ramponi, R.; Cristiani, I.; Osellame, R. Optofluidic integrated cell sorter fabricated by femtosecond lasers. *Lab Chip* **2012**, *12*, 3779–3784. [CrossRef]
9. Vitali, V.; Nava, G.; Zanchetta, G.; Bragheri, F.; Crespi, A.; Osellame, R.; Bellini, T.; Cristiani, I.; Minzioni, P. Integrated optofluidic chip for oscillatory microrheology. *Sci. Rep.* **2020**, *10*, 1–11. [CrossRef] [PubMed]
10. Crespi, A.; Lobino, M.; Matthews, J.C.; Politi, A.; Neal, C.R.; Ramponi, R.; Osellame, R.; O'Brien, J.L. Measuring protein concentration with entangled photons. *Appl. Phys. Lett.* **2012**, *100*, 233704. [CrossRef]
11. Nasu, Y.; Kohtoku, M.; Hibino, Y. Low-loss waveguides written with a femtosecond laser for flexible interconnection in a planar light-wave circuit. *Opt. Lett.* **2005**, *30*, 723–725. [CrossRef]
12. Eaton, S.M.; Ng, M.L.; Osellame, R.; Herman, P.R. High refractive index contrast in fused silica waveguides by tightly focused, high-repetition rate femtosecond laser. *J. Non.-Cryst. Solids* **2011**, *357*, 2387–2391. [CrossRef]
13. Guan, J.; Liu, X.; Salter, P.S.; Booth, M.J. Hybrid laser written waveguides in fused silica for low loss and polarization independence. *Opt. Express* **2017**, *25*, 4845–4859. [CrossRef] [PubMed]
14. Eaton, S.M.; Zhang, H.; Ng, M.L.; Li, J.; Chen, W.J.; Ho, S.; Herman, P.R. Transition from thermal diffusion to heat accumulation in high repetition rate femtosecond laser writing of buried optical waveguides. *Opt. Express* **2008**, *16*, 9443–9458. [CrossRef]
15. Arriola, A.; Gross, S.; Jovanovic, N.; Charles, N.; Tuthill, P.G.; Olaizola, S.M.; Fuerbach, A.; Withford, M.J. Low bend loss waveguides enable compact, efficient 3D photonic chips. *Opt. Express* **2013**, *21*, 2978–2986. [CrossRef]
16. Corrielli, G.; Atzeni, S.; Piacentini, S.; Pitsios, I.; Crespi, A.; Osellame, R. Symmetric polarization-insensitive directional couplers fabricated by femtosecond laser writing. *Opt. Express* **2018**, *26*, 15101–15109. [CrossRef]
17. Meany, T.; Gross, S.; Jovanovic, N.; Arriola, A.; Steel, M.; Withford, M.J. Towards low-loss lightwave circuits for non-classical optics at 800 and 1550 nm. *Appl. Phys. A* **2014**, *114*, 113–118. [CrossRef]
18. Crespi, A.; Osellame, R.; Ramponi, R.; Bentivegna, M.; Flamini, F.; Spagnolo, N.; Viggianiello, N.; Innocenti, L.; Mataloni, P.; Sciarrino, F. Suppression law of quantum states in a 3D photonic fast Fourier transform chip. *Nat. Commun.* **2016**, *7*, 1–8. [CrossRef]

19. Corrielli, G.; Crespi, A.; Osellame, R. Femtosecond laser micromachining for integrated quantum photonics. *Nanophotonics* **2021**, *10*, 3789–3812. [CrossRef]
20. Martinod, M.A.; Norris, B.; Tuthill, P.; Lagadec, T.; Jovanovic, N.; Cvetojevic, N.; Gross, S.; Arriola, A.; Gretzinger, T.; Withford, M.J.; et al. Scalable photonic-based nulling interferometry with the dispersed multi-baseline GLINT instrument. *Nat. Commun.* **2021**, *12*, 1–11. [CrossRef]
21. Riesen, N.; Gross, S.; Love, J.D.; Sasaki, Y.; Withford, M.J. Monolithic mode-selective few-mode multicore fiber multiplexers. *Sci. Rep.* **2017**, *7*, 1–9. [CrossRef]
22. Douglass, G.; Dreisow, F.; Gross, S.; Withford, M. Femtosecond laser written arrayed waveguide gratings with integrated photonic lanterns. *Opt. Express* **2018**, *26*, 1497–1505. [CrossRef] [PubMed]
23. Crespi, A.; Osellame, R.; Bragheri, F. Femtosecond-laser-written optofluidics in alumino-borosilicate glass. *Opt. Mater. X* **2019**, *4*, 100042. [CrossRef]
24. Vishnubhatla, K.C.; Bellini, N.; Ramponi, R.; Cerullo, G.; Osellame, R. Shape control of microchannels fabricated in fused silica by femtosecond laser irradiation and chemical etching. *Opt. Express* **2009**, *17*, 8685–8695. [CrossRef] [PubMed]
25. Matsuo, S.; Sumi, H.; Kiyama, S.; Tomita, T.; Hashimoto, S. Femtosecond laser-assisted etching of Pyrex glass with aqueous solution of KOH. *Appl. Surf. Sci.* **2009**, *255*, 9758–9760. [CrossRef]
26. Bischof, D.; Kahl, M.; Michler, M. Laser-assisted etching of borosilicate glass in potassium hydroxide. *Opt. Mater. Express* **2021**, *11*, 1185–1195. [CrossRef]